General Disclaimer

One or more of the Following Statements may affect this Document

- This document has been reproduced from the best copy furnished by the organizational source. It is being released in the interest of making available as much information as possible.

- This document may contain data, which exceeds the sheet parameters. It was furnished in this condition by the organizational source and is the best copy available.

- This document may contain tone-on-tone or color graphs, charts and/or pictures, which have been reproduced in black and white.

- This document is paginated as submitted by the original source.

- Portions of this document are not fully legible due to the historical nature of some of the material. However, it is the best reproduction available from the original submission.

SEMIANNUAL REPORT FOR

Grant No. NAG 1-500

SEMICONDUCTOR SUPERLATTICE PHOTODETECTORS

July 1, 1984 to December 31, 1984

Submitted to

Dr. Charles E. Byvik

FED M/S 283
National Aeronautics and Space Administration
Langley Research Center, Hampton, VA 23665

Prepared by

S. L. Chuang

Department of Electrical and Computer Engineering
University of Illinois at Urbana-Champaign
Urbana, IL 61801

and

K. Hess, J. J. Coleman, and J. P. Leburton

Department of Electrical and Computer Engineering
and
Coordinated Science Laboratory
University of Illinois at Urbana-Champaign
Urbana, IL 61801

TABLE OF CONTENTS

I. INTRODUCTION

The research grant NAG 1-500 entitled "Semiconductor Superlattice Photodetectors" was awarded to the University of Illinois by NASA-Langley Research Center on June 27, 1984. Dr. Charles E. Byvik of NASA is the Technical Officer, and Mr. John F. Royall is the Grants Officer. The total amount of funds received by the University is $62,801 to cover the period from July 1, 1984 to June 30, 1985.

This report is the first semiannual report.

1. Period

July 1, 1984 to December 31, 1984.

2. Reporting Date

January 5, 1985.

3. Technical Personnel

S. L. Chuang: Assistant Professor of Electrical and Computer Engineering and TRW Assistant Professor of Electrical and Computer Engineering

J. J. Coleman: Professor of Electrical and Computer Engineering and Research Professor of Coordinated Science Laboratory

K. Hess: Professor of Electrical and Computer Engineering and Research Professor of Coordinated Science Laboratory

J. P. Leburton: Assistant Professor of Electrical and Computer Engineering and Research Assistant Professor of Coordinated Science Laboratory

Peter J. Mares: Research Assistant of Electrical and Computer Engineering

II. TECHNICAL PROGRESS

The advent of Molecular Beam Epitaxy (MBE) and Metalorganic Chemical Vapor Deposition (MOCVD) makes possible the construction of devices with enormous geometrical sophistication. The solid state analog of a photomultiplier becomes in the technological course of these developments a realistic possiblility and we show that theoretical considerations support the feasibility and superiority of such a device.

In the past six-month period, we studied two novel types of superlattice photodetectors: (1) a superlattice photomultiplier and (2) a photodetector based on the real space transfer mechanism. The wavelength for the first device is of the order of micron or flexible corresponding to the bandgap absorption in a semiconductor. The wavelength for the second device is in the micron range (about 2 to 12 microns) corresponding to the energy of the conduction band edge discontinuity between an $Al_xGa_{1-x}As$ and GaAs interface.

1. Superlattice Photomultiplier

This device consists of alternating $Al_xGa_{1-x}As$ and GaAs layers where the GaAs layers are heavily doped with donors (Figure 1). The electrons freed from the donors are essentially confined within the quantum wells. Optically generated electrons are accelerated by the external field and bombard the electrons confined in the wells. Thus this device is based on a mechanism similar to the conventional photomultiplier.

The detailed theoretical formulations are shown in the Appendix. We summarize our approach and present numerical results here. The incident light is absorbed in the first $Al_xGa_{1-x}As$ layer (or other material) across the bandgap with the energy gap E_g given by [1]. The electrons generated by the optical injection are then accelerated and interact with the electrons in the quantum

wells (Figure 1). The wave functions for the incident electrons and the confined electrons are used to calculate the electron-electron interaction due to Coulomb force with screening effects taken into account [2] - [6]. The quantum mechanical transition rate for a system involving an initial state of one free electron and one bound electron in the well and a final state of both electrons free is calculated using the matrix element for electron-electron interaction (Figure 2). The average scattering rate over the momentum (energy) distributions of all electrons is then calculated. The average scattering time is then obtained from the inverse of the scattering rate per incident electron, the calculation of which is similar to that for Auger time constants [7], [8].

We have calculated the average time constant for various cases. In Figure 3, we plot the average time constant versus the doping concentration in the GaAs layer, N_D. Both are in logarithmic scales. The solid line is for $T_e/T = 2$, and the dashed line is for $T_e/T = 3$. The quantum well size is $L_z = 400$ Å, and $L = 800$ Å. The time constant is of the order of 10 picoseconds in the figure. We see that the ionization time constant decreases as the electron temperature is increased, i.e., as the electric field is increased. This is expected since increasing the electric fields will create more hot electrons which have enough energy to ionize the bound electrons in the quantum well region. From the figure, we also see that the ionization process becomes faster when the donor concentration is increased. The reason is that more electrons are available in the quantum well region and the Fermi level is increased with the donor concentration

In Figure 4, the results are shown for different dimensions of the quantum wells: $L_z = 360$ Å, $L = 720$ Å. The average time constant decreases because thinner quantum wells will have higher ground energy levels. Thus the energy required for the bound electrons to become free becomes smaller, and the impact

ionization process becomes faster. Similar to the previous figure, the average time constant is decreased as the electron temperature is increased. In Figure 5, the lattice temperature is increased to room temperature. We plot two cases for $T_e/T = 1$ (solid line) and $T_e/T = 2$ (dashed line). For the same range of the carrier concentrations, the electron-electron interaction is faster at room temperature than that at 77K. That is because the electron distribution as a function of energy is broader at higher temperature, there are more electrons with enough energy to impact ionize the bound electrons.

The internal gain of the device can be estimated as follows. The gain for each period L between two adjacent layers is due to the ionized electrons. Thus (Figure 1)

$$\Delta n = n_{\ell+1} - n_\ell \equiv n_\ell \langle \frac{1}{\tau} \rangle \Delta t$$

where $\langle \frac{1}{\tau} \rangle$ is the average scattering rate due to electron-electron interaction, as calculated from the Appendix A and the reciprocal of $\langle \frac{1}{\tau} \rangle$ has been shown in Figures 3-5. Δt is the average traveling time for an electron in a distance L.

$$\Delta t = \frac{L}{\langle v \rangle}$$

where $\langle v \rangle$ is the average drift velocity. Thus

$$\frac{n_{\ell+1}}{n_\ell} = 1 + \langle \frac{1}{\tau} \rangle \frac{L}{\langle v \rangle}$$

which is the gain in one period L.

The overall gain of the device, if there are N periods, will be

$$G = \left(1 + \langle \frac{1}{\tau} \rangle \frac{L}{\langle v \rangle} \right)^N$$

For example, from Figure 4, at a doping concentration $N_D = 1 \times 10^{16} cm^{-3}$, and $T_e/T = 3$ (dashed line), the average time constant is 4.38 psec. Assuming

$\langle v \rangle \approx 10^6$ cm/sec, we have the gain $G = (2.6438)^N$. If there are 10 layers, we obtain a gain of 1.67×10^4. If $\langle v \rangle = 10^7$ cm/sec, $G \approx 4.6$ for $N = 10$; and $G = 21$ for $N = 20$.

From the above analysis, we see that there are a few advantages in this device. (1) The gain is in a discretized fashion over each period rather than distributed as in the conventional avalanche photodetectors. (2) The response time of the device can be very fast and is estimated to range from as short as a picosecond to as long as a nanosecond. Future study on the noise property of this device will be useful.

2. A Superlattice Photodetector Based on Real Space Transfer Mechanism

As shown in Figure 6, a photodetector based on the real space transfer mechanism [9], [10] is studied. Before the detector is exposed to the optical signal, the electrons are conducting in the quantum well region parallel to the $A\ell_xGa_{1-x}As$ - GaAs boundary. The mobility in the GaAs region is higher than that in the $A\ell_xGa_{1-x}As$ layer. When the device is under optical illumination, the electrons absorb the optical energy and most of them will conduct in the $A\ell_xGa_{1-x}As$ region where the mobility of the electron is low. Thus there is a change in the conductivity of the device. This real space transfer mechanism has been studied for its negative differential conductivity [11], and its fast switching and storage properties [12]. We have started investigating its optical applications. The optical absorption coefficient can be calculated from the free carrier absorption, which is based on the second order time-dependent perturbation theory since the phonon is involved in the photon absorption process. The electron bound by the quantum well may absorb a photon first and then either absorb a phonon or emit a phonon for the momentum conservation. We have formulated the second-order transition rate and will calculate the absorption coefficient. The detection wavelength is in the micron range (2 to 12 microns)

corresponding to the conduction band edge discontinuity ΔE_c.

$$\Delta E_c = 85o/o * \Delta E_g^{\Gamma} = 1.06\ x$$

for $0 < x < 0.45$, where x is the mole fraction for AℓAs in the $A\ell_x Ga_{1-x}As$ region. ΔE_g^{Γ} is the energy gap difference between the two regions and can be obtained from ref. [1].

Thus for the atomic fraction $x = 0.1$, $\Delta E_c = 0.106$ eV, and the corresponding wavelength for absorption is about 12 microns. If $x = 0.45$, $\Delta E_c = 0.477$ eV, and the absorption wavelength is 2.6 microns. The photoconductivity for this device will be calculated taking into account the real space transfer mechanism.

APPENDIX A

THEORETICAL FORMULATIONS OF THE ELECTRON-ELECTRON INTERACTION IN A SUPERLATTICE PHOTOMULTIPLIER

In this Appendix, we show the derivations for the electron-electron interaction in a superlattice photomultiplier. Consider an incident free electron interacting with a bound electron in a quantum well; the total average transition rate per unit volume P_{tr} is given by

$$P_{tr} = \frac{1}{V} \sum_{\vec{k}_1} \sum_{\vec{k}_2} \sum_{\vec{k}_1'} \sum_{\vec{k}_2'} P_{\vec{k}_1\vec{k}_2}^{\vec{k}_1'\vec{k}_2'} f(\vec{k}_1)\, f(\vec{k}_2)\, [1 - f(\vec{k}_1')][1 - f(\vec{k}_2')] \tag{A1}$$

where $P_{\vec{k}_1\vec{k}_2}^{\vec{k}_1'\vec{k}_2'}$ is the quantum mechanical transition rate (number per second) between the initial state of electron 1 in state $\vec{k}_1$, electron 2 in state $\vec{k}_2$ and the final state of electron 1 in state $\vec{k}_1'$ and electron 2 in state $\vec{k}_2'$ (Fig. 2). f is the Fermi-Dirac distribution.

$$P_{\vec{k}_1\vec{k}_2}^{\vec{k}_1'\vec{k}_2'} = \frac{2\pi}{\hbar} |\langle 12|H_s|1'2'\rangle|^2\, \delta(E_1 + E_2 - E_1' - E_2') \tag{A2}$$

where the matrix element $|\langle 12|H_s|1'2'\rangle|^2$ is given by

$$|\langle 12|H_s|1'2'\rangle|^2 = 4 \left| \int \psi_{\vec{k}_1}^{*}(\vec{r}_1)\, \psi_{\vec{k}_2}^{*}(\vec{r}_2)\, \frac{e^2 \exp(-q|\vec{r}_1 - \vec{r}_2|)}{4\pi\, \varepsilon\, |\vec{r}_1 - \vec{r}_2|}\, \psi_{\vec{k}_1'}(\vec{r}_1)\, \psi_{\vec{k}_2'}(\vec{r}_2)\, d\vec{r}_1 d\vec{r}_2 \right|^2 \tag{A3}$$

and

$$|12\rangle \equiv \psi_{\vec{k}_1}(\vec{r}_1)\, \psi_{\vec{k}_2}(\vec{r}_2)$$

$$= \frac{\exp(i\vec{k}_1 \cdot \vec{r}_1)}{\sqrt{V}} \cdot \sqrt{\frac{2}{AL_z}} \exp(i\vec{k}_{2t} \cdot \vec{r}_{2t}) \sin \frac{n\pi}{L_z} z_2 \tag{A4}$$

$$|1'2'\rangle \equiv \psi_{\vec{k}_1'}(\vec{r}_1)\ \psi_{\vec{k}_2'}(\vec{r}_2)$$

$$= \frac{\exp(i\vec{k}_1'\cdot\vec{r}_1)}{\sqrt{V}} \frac{\exp(i\vec{k}_2'\cdot\vec{r}_2)}{\sqrt{V}} \tag{A5}$$

where $\vec{k}_1$, $\vec{k}_1'$, $\vec{k}_2'$, $\vec{r}_1$, $\vec{r}_2$ are the general three-dimensional vectors and $\vec{k}_{2t}$, $\vec{r}_{2t}$ are two-dimensional vectors.

$$\vec{k}_2^{\pm} = \vec{k}_{2t} \pm \hat{z}\frac{n\pi}{L_z} = \hat{x}k_x + \hat{y}k_y \pm \hat{z}\frac{n\pi}{L_z} \tag{A6}$$

$$\vec{r}_2 = \vec{r}_{2t} + \hat{z}z_2 = \hat{x}x_2 + \hat{y}y_2 + \hat{z}z_2 \tag{A7}$$

Here $\vec{k}_2^{\pm}$ are defined because $\sin(\frac{n\pi}{L_z} z_2)$ can be decomposed into the sum of two exponential functions with $(+\frac{n\pi}{L_z})$ and $(-\frac{n\pi}{L_z})$ in the arguments.

Replacing the summations $\sum_{\vec{k}}$ by integrations, i.e.,

$$\sum_{k} = \frac{V}{(2\pi)^3}\int d\vec{k} \tag{A8}$$

for $\vec{k}_1$, $\vec{k}_1'$ and $\vec{k}_2'$, and

$$\sum_{\vec{k}_2} = \frac{A}{(2\pi)^2}\int d\vec{k}_{2t} \tag{A9}$$

since the z-component of $\vec{k}_2$ is quantized in the quantum well, and we assume only one energy level, we obtain

$$P_{tr} = \frac{e^4}{\epsilon^2}\frac{4\pi}{\hbar}\left(\frac{L_z}{L}\right)^2 \int \frac{d\vec{k}_1}{(2\pi)^3} f(\vec{k}_1) \int \frac{d\vec{k}_{2t}}{(2\pi)^2 L_z}\left[S(\vec{k}_1,\vec{k}_2^{+}) + S(\vec{k}_1,\vec{k}_2^{-})\right] \tag{A10}$$

where

$$S(\vec{k}_1, \vec{k}_2^{\pm}) = \int d\vec{k}_1' \frac{\delta(E_1 + E_2 - E_1' - E_2')}{[\,|\vec{k}_1 - \vec{k}_1'|^2 + q^2\,]^2}$$

$$= \frac{m^*}{\hbar^2 q^2} \frac{|\vec{k}_1 - \vec{k}_2^{\pm}|}{|\vec{k}_1 - \vec{k}_2^{\pm}|^2 + q^2} \qquad \text{(A11)}$$

where momentum conservation $\vec{k}_2' = \vec{k}_1 + \vec{k}_2^{\pm} - \vec{k}_1'$ has been used in the above derivations.

Assume that the incident electron 1 has a Maxwellian-Boltzmann distribution in the region $Al_xGa_{1-x}As$ before it hits the interface,

$$f(\vec{k}_o) = 4 \left(\frac{\pi h^2}{2m^* kT_e}\right)^{3/2} n_1 \exp[-E(\vec{k}_o)/kT_e] \qquad \text{(A12)}$$

where T_e is the electron temperature of the hot electrons.

$$E(\vec{k}_o) = \frac{h^2}{2m^*} (k_{ox}^2 + k_{oy}^2 + k_{oz}^2) \quad . \qquad \text{(A13)}$$

Here k_{oz} is the z-component of the $\vec{k}$ vector of electron 1 in the $Al_xGa_{1-x}As$ region and is related to k_{1z} by

$$k_{oz} = \sqrt{k_{1z}^2 - \frac{2m^*}{\hbar^2} \Delta E_c} \qquad \text{(A14)}$$

and

$$k_{ox} = k_{1x} \qquad \text{(A15)}$$

$$k_{oy} = k_{1y} \qquad \text{(A16)}$$

from both the energy conservation and the boundary conditions, where we have assumed that the effective mass m^* is unchanged for simplicity.

The average scattering rate is given by the integration over $d\vec{k}_o$ instead of $d\vec{k}_1$,

$$\left\langle \frac{1}{\tau} \right\rangle = \frac{P_{tr}}{n_1} = 2 \int_{k_{oz}=k_{th}}^{\infty} \int_{-\infty}^{\infty} \int_{-\infty}^{\infty} \frac{dk_{ox} dk_{oy} dk_{oz}}{(2\pi)^3} f(\vec{k}_o) \left\langle \frac{1}{\tau(k_1)} \right\rangle \tag{A17}$$

where

$$\left\langle \frac{1}{\tau(\vec{k}_1)} \right\rangle = \frac{1}{n_1} \frac{4\pi e^4}{\epsilon^2 \hbar} \left(\frac{L_z}{L} \right)^2 \int \frac{d\vec{k}_{2t}}{(2\pi)^2 L_z} [S(\vec{k}_1, \vec{k}_2^{+}) + S(\vec{k}_1, \vec{k}_2^{-})] \quad . \tag{A18}$$

Since $f(\vec{k}_o)$ achieves its maximum at $k_{ox} = 0$, $k_{oy} = 0$, we can evaluate dk_{ox}, dk_{oy} integrations in closed-form by approximating

$$\left\langle \frac{1}{\tau(\vec{k}_1)} \right\rangle \simeq \left\langle \frac{1}{\tau(\vec{k}_1)} \right\rangle_{\substack{k_{ox}=0 \\ k_{oy}=0}} \tag{A19}$$

and carry out the integrations. The final integral for dk_{oz} is done numerically by Simpson's rule. The threshold wave vector k_{th} is given by

$$k_{th} = \sqrt{\frac{2m^*}{\hbar^2} (\Delta E_c - E_1)} \tag{A20}$$

i.e., from the minimum energy required for both electrons to be free from the quantum well. The average time constant is obtained immediately by the reciprocal of the scattering rate, i.e., $\left\langle \frac{1}{\tau} \right\rangle^{-1}$.

REFERENCES

[1] H. C. Casey, Jr. and M. B. Panish, Heterostructure Lasers. New York: Academic Press, 1978.

[2] J. M. Ziman, Electrons and Phonons. London: Oxford University Press, Amen House, 1960.

[3] A. R. Beattie and P. T. Landsberg, "Auger effect in semiconductors," Proc. R. Soc. London, vol. A249, pp. 16-29, 1959.

[4] P. T. Landsberg, C. Phys-Roberts and P. Lal, "Auger recombination and impact ionization involving traps in semiconductors," Proc. Phys. Soc. London, vol. 84, pp. 915-931, 1964.

[5] A. R. Beattie and G. Smith, "Recombination in semiconductors by a light hole Auger transition," Phys. Status Solidi, vol. 19, pp. 577-586, 1967.

[6] P. T. Landsberg, "Non-radiative transitions in semiconductors," Phys. Status Solidi, vol. 41, pp. 457-489, 1970.

[7] M. Takeshima, "Auger recombination in InAs, GaSb, InP, and GaAs," J. Appl. Phys., vol. 43, pp. 4114-4119, 1972.

[8] A. Sugimura, "Auger recombination effect on threshold current of InGaAsP quantum well lasers," IEEE J. Quantum Electron., vol. QE-19, pp. 932-941, 1983.

[9] H. Shichijo, K. Hess and B. G. Streetman, "Real space electron transfer by thermionic emission in GaAs-$Al_xGa_{1-x}As$ heterostructures: analytical model for large layer widths," Solid-State Electron., vol. 23, pp. 817-822, 1980.

[10] K. Hess, B. G. Streetman and H. Morkoc, "Negative resistance heterojunction Devices, U. S. Patent No. 4257055, March 1981.

[11] K. Hess, H. Morkoc, H. Shichijo, and B. G. Streetman, "Negative differential resistance through real-space electron transfer," Appl. Phys. Lett., vol. 35, pp. 469-471, 1979.

[12] M. Keever, K. Hess and M. Ludowise, "Fast switching and storage in GaAs-$Al_xGa_{1-x}As$ heterojunction layers," IEEE Trans. Electron. Devices Lett., vol. EDL-3, pp. 297-300, 1982.

FIGURE CAPTIONS

Figure 1. Geometrical configuration for a superlattice photomultiplier.

Figure 2. The initial and final states for the electron-electron interaction used in the photomultiplication process.

Figure 3. The average time constant versus the doping concentration N_D for two electron temperatures at T = 77K.

Figure 4. The average time constant versus the doping concentration N_D for two electron temperatures. The quantum well size is different from that of Figure 3.

Figure 5. The average time constant versus the doping concentration for two electron temperatures T_e at T = 300K.

Figure 6. (a) Photodetectors using real space transfer mechanism.
(b) When no light is injected, electrons conduct in GaAs layers, where their mobility is large.
(c) With light injection, electrons conduct in $A\ell_xGa_{1-x}As$ layers, where their mobility is small.

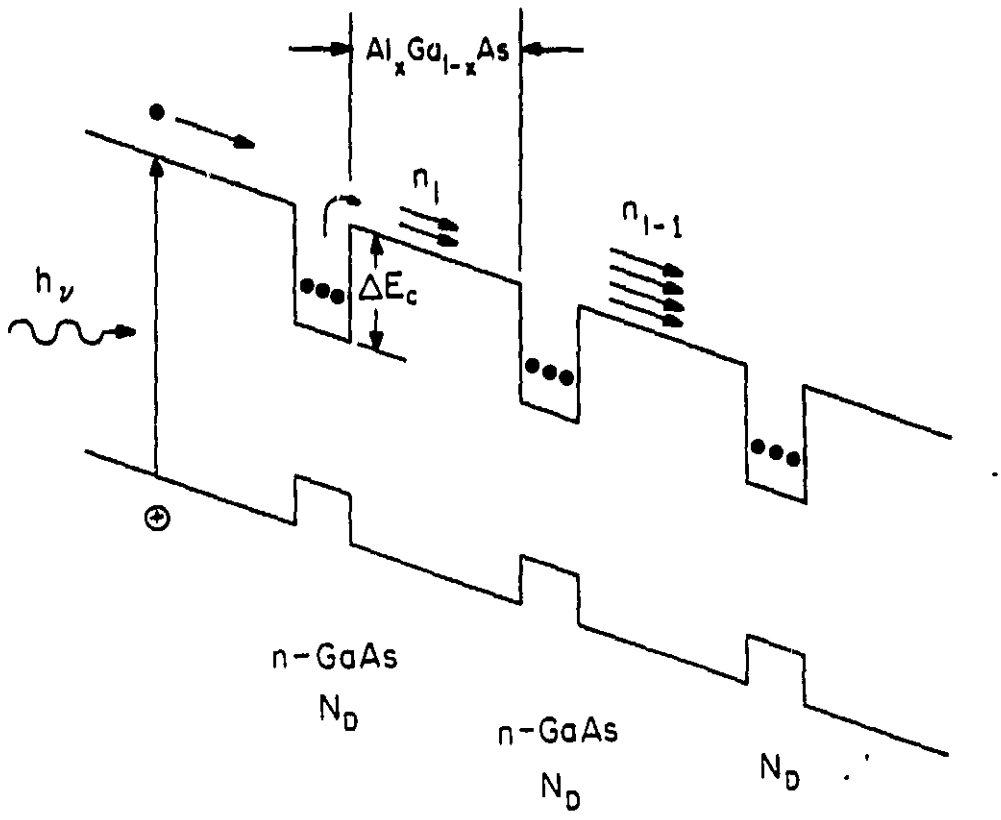

Figure 1. Geometrical configuration for a superlattice photomultiplier.

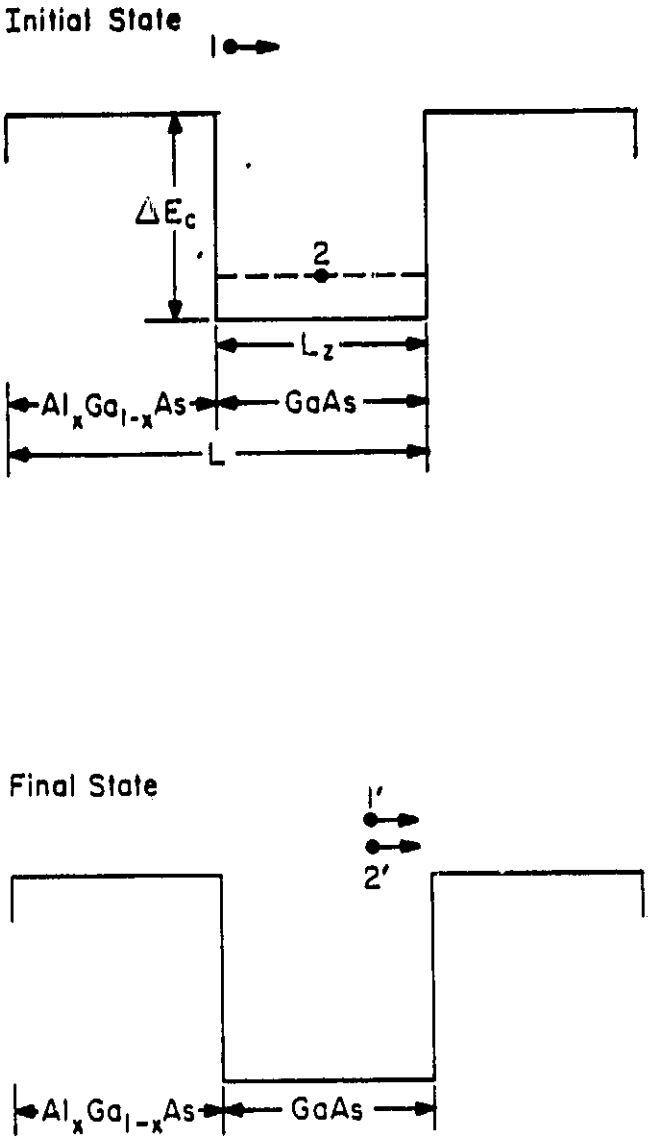

Figure 2. The initial and final states for the electron-electron interaction used in the photomultiplication process.

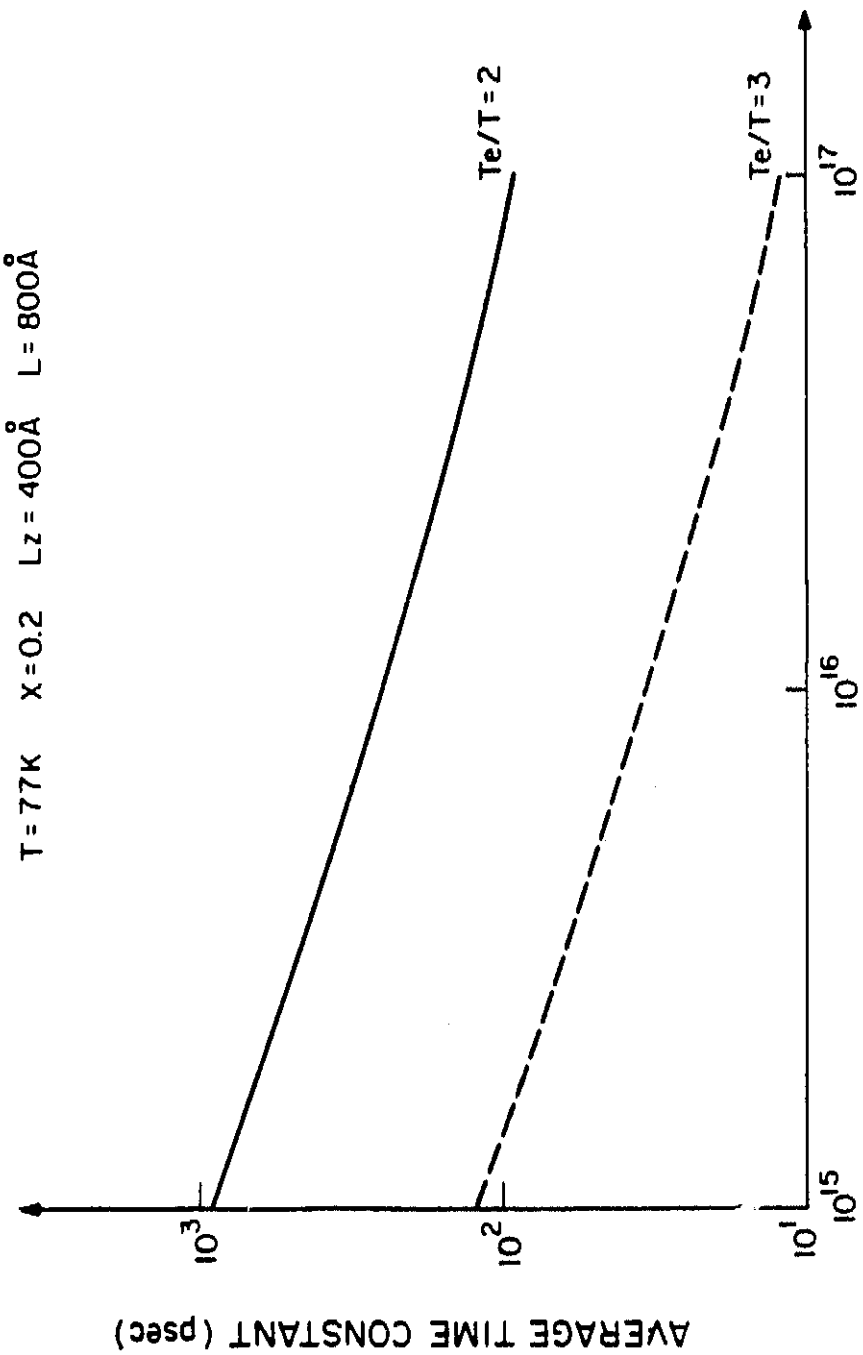

Figure 3. The average time constant versus the doping concentration N_D for two electron temperatures at T = 77K.

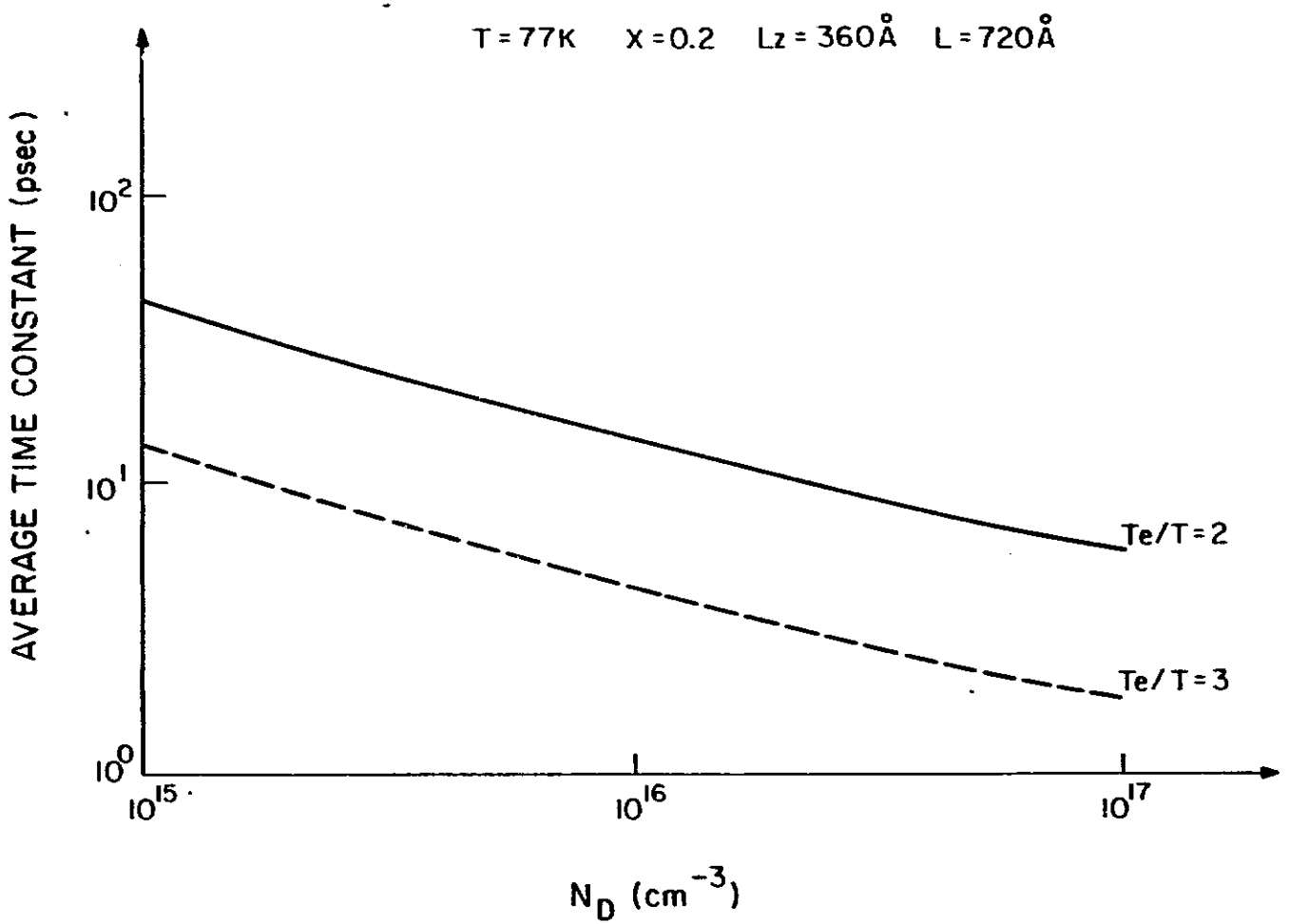

Figure 4. The average time constant versus the doping concentration N_D for two electron temperatures. The quantum well size is different from that of Figure 3.

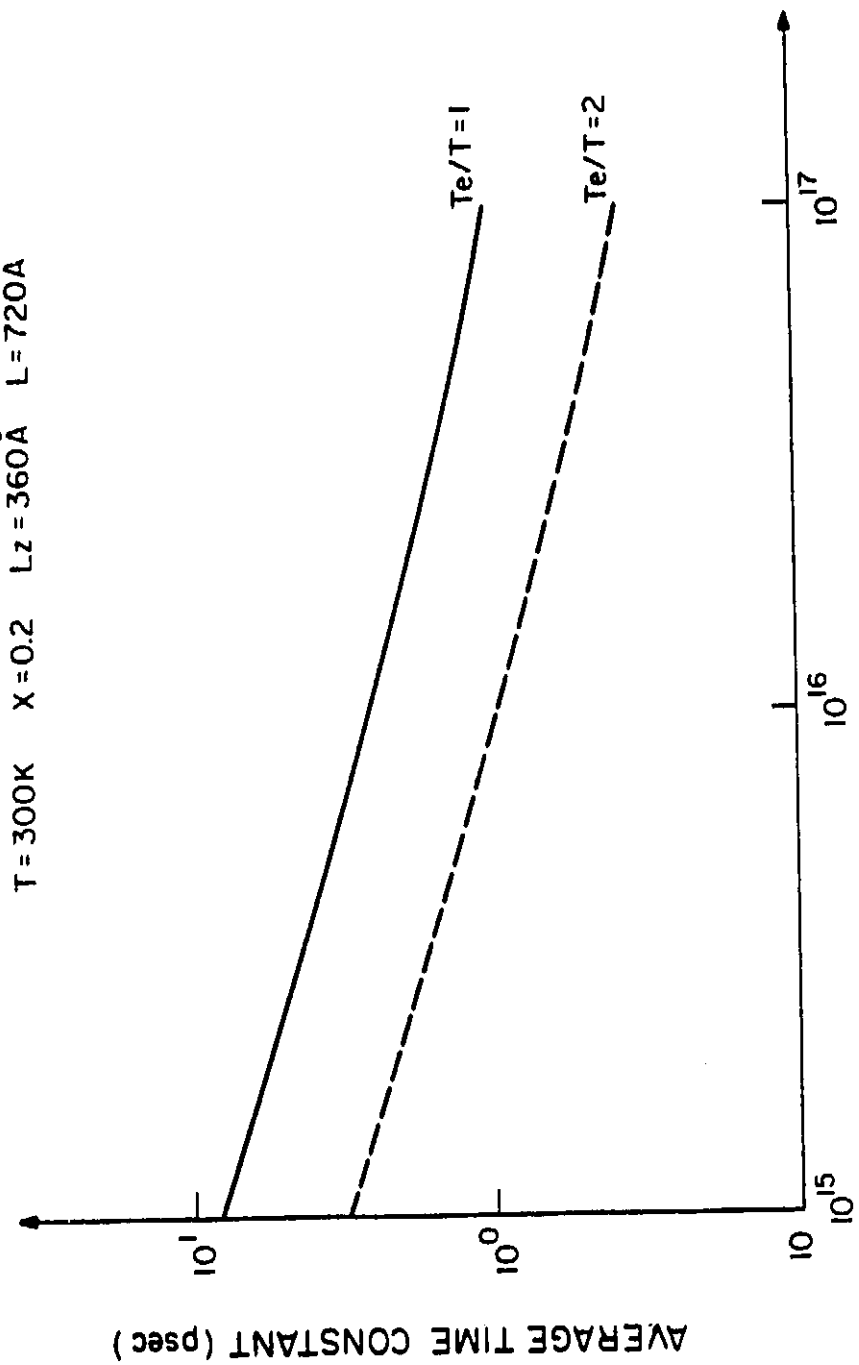

Figure 5. The average time constant versus the doping concentration for two electron temperatures T_e at T = 300K.

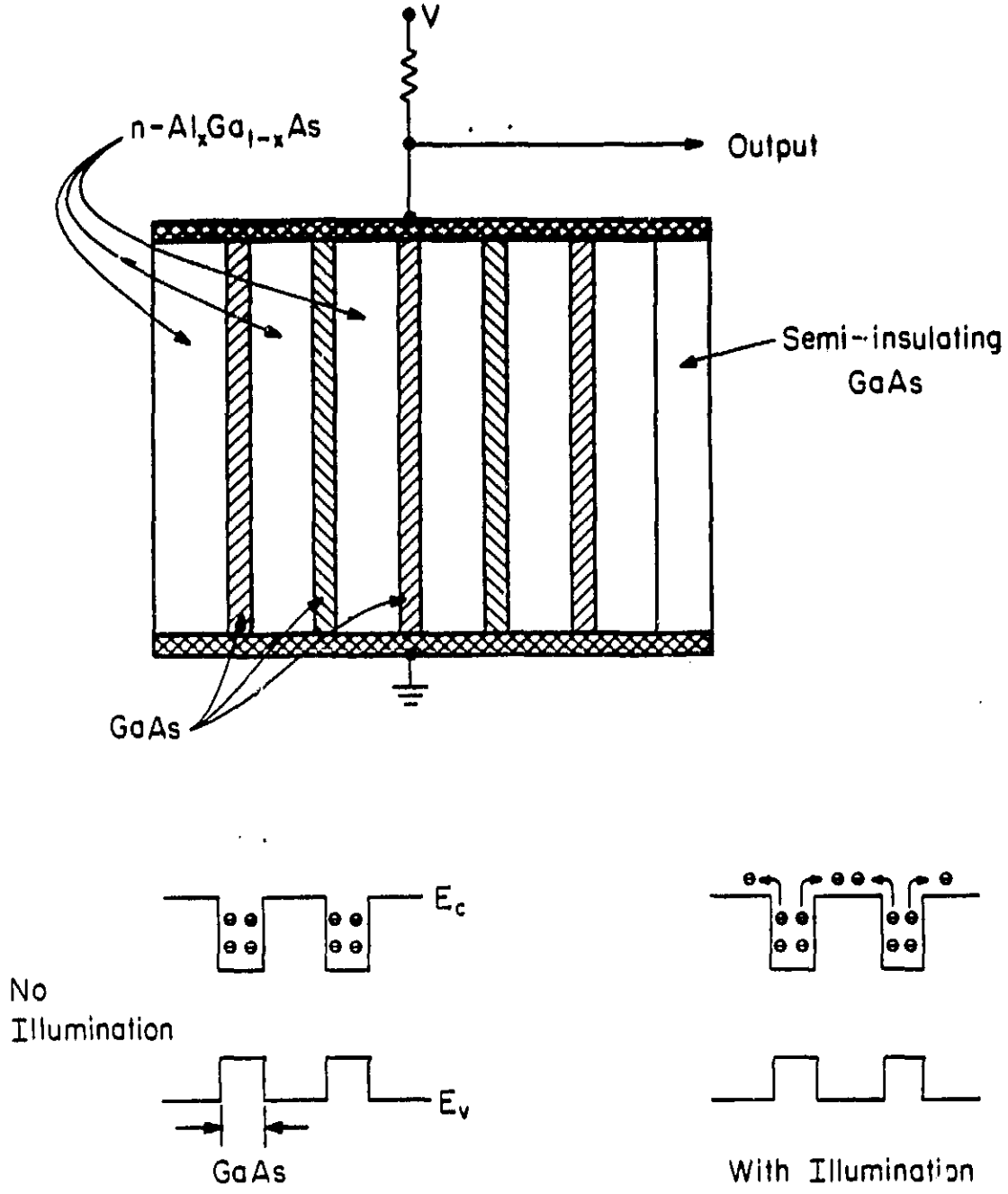

Figure 6. (a) Photodetectors using real space transfer mechanism.
(b) When no light is injected, electrons conduct in GaAs layers, where their mobility is large.
(c) With light injection, electrons conduct in $Al_xGa_{1-x}As$ layers, where their mobility is small.